Spectroscopic study of lithiumlike carbon by dielectronic recombination of a stored ion beam

S. Mannervik, S. Asp, L. Broström, D. R. DeWitt, J. Lidberg, and R. Schuch
Atomic Physics, Stockholm University, S-104 05 Stockholm, Sweden

K. T. Chung
Department of Physics, North Carolina State University, Raleigh, North Carolina 27695-8202

(Received 2 October 1996)

A detailed spectroscopic study of resonant states in the continuum of lithiumlike carbon has been performed utilizing dielectronic recombination at an ion storage ring. All observed resonances have been identified and energies have been determined with an accuracy better than 0.1 eV. The measurements have been complemented by accurate calculations using the saddle-point technique. Every resonance of the type $1snln'l'$ has been determined for $n=2$, $n'=2,3$). [S1050-2947(97)01203-1]

PACS number(s): 32.30.Rj, 34.80.Lx, 31.15.Pf

I. INTRODUCTION

As far back as 1939, the spectroscopists Edlén and Tyrén [1] reported an observation of ''atomic energy states of an unusual type'' in carbon. They had observed spectral lines in their vacuum spark spectra that did not fit into the ordinary energy-level systems. The strongest features had wavelengths about 1 Å longer than the resonance transition ($1s^2\,{}^1S-1s2p\,{}^1P$) in heliumlike carbon at 40.27 Å. They proposed that the observed lines originated from radiative decay of doubly excited states (e.g., $1s^22s-1s2s2p$). This was a remarkable observation, which was given the following explanation by Edlén and Tyrén [1]: ''one must assume the existence of discrete energy levels lying *above* the ionization limits by amounts up to *five times* the ionization potentials of the same spectrum.''

In the case of carbon, the observation indicated the existence of narrow discrete states in the continuum at energies about 240 eV above the ionization limit. The existence of such narrow discrete states (i.e., nonautoionizing states) can be understood in terms of quantum-mechanical selection rules as follows. Autoionization is primarily mediated by the Coulomb interaction. In this process the total angular momentum J and the parity π of the total wave function are conserved. When the fine-structure interaction is weak on the relative scale and the LS-coupling approximation is good, the angular momentum L and the total spin S will also be conserved separately. The continuum above the ionization limit $1s^2$ will consequently be restricted to certain symmetries and not until energies are reached that lie above the energy of $1s2p\,{}^3P$ in the next ionization state will all symmetry combinations be available. For instance, the $1s2p^2\,{}^2P$ state of even parity is embedded in the continuum $1s^2\epsilon p\,{}^2P$ of odd parity, which indicates that this is a quasibound state that decays by radiative decay instead of autoionization. Similarly, all quartet states below $1s2s\,{}^3S$ will act as bound states since autoionization by the Coulomb interaction is forbidden and autoionization by relativistic effects is negligible. These states can consequently be observed in radiative transitions.

It was found early that the beam-foil technique was an efficient tool for producing multiply excited states. Term systems of many low-Z Li-like systems have been constructed from such measurements. An extensive review article by Mannervik [2] summarizes these results. The doubly excited quartets in Li-like carbon have been studied by Dumont *et al.* [3] and Blanke *et al.* [4]. Some optical spectroscopic observations of transitions of the kind Edlén and Tyrén observed, have been reported more recently [5–7]. It is also possible to observe autoionizing states in radiative transitions since such transitions are in general competing decay channels. Usually the branching ratio for radiative decay is small and consequently the optical line intensity will be weak. On the other hand, optical measurements will normally give high accuracy. Levels in doubly excited C IV determined by optical methods have been determined with an accuracy better than 100 meV on an absolute scale.

While the quasibound states in the continuum can be accurately determined, the autoionizing states are harder to determine accurately with experimental methods. A natural method here is the study of the Auger spectra of the ions. Examples of such measurements are the high-energy collision studies by Schneider *et al.* [8] and by Rødbro *et al.* [9] as well as the experiment at lower collision energy by Mann [10]. From these high-resolution Auger spectra, energies were determined with an accuracy of typically 0.5 eV and 0.2 eV, respectively. Another method to measure energies of the autoionizing states is by studies of the dielectronic recombination (DR) process, in which the autoionizing states are populated by the inverse process of autoionization. After radiative stabilization the recombination is completed. This method was used for carbon by Andersen *et al.* [11] in a single-pass experiment in which an energy resolution of 0.135 eV was obtained. They did not, however, determine absolute energies in this case. In a more recent DR experiment at the ion storage ring TSR in Heidelberg, Kilgus *et al.* [12] determined energies of resonant states with uncertainties in the range 0.1–0.8 eV. The resolution in these experiments is set by the electron target temperature. The energy resolution obtained by Kilgus *et al.* was about 2 eV. In more recent experiments in the storage ring CRYRING in Stockholm, the energy resolution was improved by almost one order of magnitude to 0.3 eV (at collision energies of about 40 eV)

[13,14], opening opportunities to improve the carbon measurements substantially.

Doubly excited three-electron systems are challenging objects for testing high-accuracy calculations. With three open shells, there is much correlation, but still only three electrons to treat. Thus these systems are ideal for advanced treatment. For the quasibound states very accurate calculations have been performed reaching accuracies 1 meV and better. A good example is the $1s2s2p\ ^4P$ state in neutral lithium for which a very accurate energy was obtained by Bunge [15] and later by Chung [16]. More comparisons between accurate calculations and experiments are given in the review article by Mannervik [2]. For autoionizing states, for which no upper bound principle in the variational procedure can be used, the accuracy has been orders of magnitude lower. Since experiments have rarely determined energies to better than with about 1 eV, there has been no real challenge for theory. Now, however, more accurate experiments give incentive for more accurate calculations for autoionizing states. In particular, the saddle-point technique introduced by Chung [17] has proven to be a powerful method to obtain accurate results (see, e.g., [2]).

In this work we present an accurate experimental investigation of the excitation energies of the spectrum of autoionizing states in Li-like carbon. Complementing these results, we also present energy values from accurate calculations.

II. EXPERIMENT

The C^{4+} ions were produced by an electron-beam ion source and preaccelerated to 300 keV/amu in a radio frequency quadrupole before injection into the ring. The ions were accelerated to their final energy of 11 MeV/amu in the synchrotron-storage ring CRYRING [18]. The ions were cooled by a velocity-matched electron beam over an interaction length $l=80\pm 8$ cm. During cooling, which takes place over less than 1 s, the ion-beam diameter shrinks to roughly 1 mm full width at half maximum, decreasing the range of relative electron-ion velocities. In this measurement the ion current was $I_i=2.7\pm 0.3\ \mu$A, which corresponds to a number of $N_i\simeq 5\times 10^6$ stored ions. The beam half-life, determined by contributions from recombination in the cooler, electron capture from the background gas, and electron loss in collisions with the background gas, was approximately 130 s. The residual gas pressure in the ring was less than 10^{-11} torr.

The electron cooler doubles as a target for electron-ion interactions. In order to scan the interaction energies across DR resonances with $\Delta n=1$, the cathode voltage is ramped through values to give electron velocities both above and below the ion velocity. As described below, scanning of both sides of the ion velocity produces spectra under significantly different conditions, the analysis of which provides a means of improving the accuracy of the reported resonance energies. Following recombination, the C^{3+} ions are separated from the circulating beam in the first dipole magnet beyond the cooler and detected with a surface barrier detector with an efficiency of roughly 100%. At the present beam energy any excited C^{3+} ions with $n>n_{\max}=16$ will undergo field ionization when passing the dipole magnets and not be detected. Upon detection of a C^{3+} ion the instantaneous cathode voltage is recorded, along with the precise arrival time relative to the voltage ramp. The recorded times, generated by the ring's master timing computer, provide a higher-quality (noise-free) spectrum that is directly related to the instantaneous cathode voltage. The ion velocity is precisely determined from the Schottky frequency and the beam path length $L=51.68$ cm.

Calculation of the electron-ion interaction energies requires an accurate determination of the electron velocity, including space-charge effects. The total space charge in the interaction region of the cooler includes a contribution from trapped positive ions created by ionization of residual gases. The electron velocity v_e is related to the cathode voltage V_c and the space charge through the equation

$$E_{\rm lab}=eV_c-\left(\frac{1}{v_e}-\frac{\zeta}{v_c}\right)\frac{Ir_cm_ec^2}{e}\left[1+2\ln\left(\frac{R_t}{R_b}\right)\right], \qquad (1)$$

where $E_{\rm lab}$ is the electron energy in the interaction region, I is the electron current, v_c is the electron velocity during cooling, $\zeta(<1)$ represents the positive ion contribution, r_c is the classical electron radius, R_b $(=2$ cm) is the radius of the electron beam, and R_t $(=5$ cm) is the radius of the beam tube. During cooling the ions accelerate or decelerate to exactly match the electron velocity. The electron velocity at cooling is therefore given by the ion velocity; the initial value of ζ is determined by solving Eq. (1) once the cooling velocity is measured.

In order to scan the energy range of interest the cathode voltage was ramped both above and below the cooling voltage. During the voltage scans the population of trapped positive ions varies in relation to the space-charge variation of the electron beam. We estimated the variation of $\zeta(t)$ by modeling the ion population using a simple equation relating the rate of ion production through electron impact and the rate of loss through escape from the space charge. This model includes one adjustable parameter that may be interpreted as the local density of neutral molecules in the interaction region of the cooler. When calculating the electron energy $E_{\rm lab}(t)$ in the interaction region at a time t during the ramp, the instantaneous values of $\zeta(t)$ and $V_c(t)$ are used in Eq. (1).

Once the laboratory frame energy of the electrons has been determined, the center-of-mass interaction energy is obtained from the relativistic expression [19]

$$E_{\rm c.m.}=[(E_i+E_e+M_ic^2+m_ec^2)^2-(\sqrt{E_i^2+2M_ic^2E_i}+\sqrt{E_e^2+2m_ec^2E_e})^2]^{1/2}-M_ic^2-m_ec^2 \qquad (2)$$

for each data point, where M_i and E_i are the ion mass and energy, respectively. To check our estimates of the resonance energies we compared the positions of the peaks obtained in the high- and low-velocity (relative to the cooling velocity) spectra. We found in the present case that the two spectra could not be exactly matched for any reasonable values of the trapped ion intensity. The electron velocity is known indirectly through a series of transforms, including a conversion from an analog-to-digital converter channel to the cathode voltage and an estimate of the trapped ion population. However, there exists the possibility that any of them may contain small offsets or calibration errors. Small adjustments

of the cathode voltage through the addition of a linear shift $V_c \rightarrow V_c + A_0 + A_1 V_c$ were therefore used to bring the two spectra into agreement. The parameter A_0 may be interpreted as a power supply calibration offset, while A_1 may result from the leakage of current from the power supply to ground; such a leakage current would produce a voltage-dependent shift. These three parameters were adjusted to match the high and low spectra in accordance with three criteria: (i) the lowest energy peak in the high-side spectrum, identified as the $(2s2p\ ^3P)\ ^2P^o$ resonance, must appear at the calculated energy of 235.5 eV; (ii) the corresponding peak in the low-side spectrum must also appear at 235.5 eV; and (iii) the difference between the energy positions of the series limit must be minimized. The spectra then yield accurate energy values for the higher-energy resonances up to the series limit and the uncertainty in the energy of the series limit is given by the difference in the two values.

III. THEORY

To study the spectroscopic data utilizing dielectronic recombination, we carry out theoretical calculation for the resonances of C IV. In the energy region between 220 and 285 eV, we expect the C IV resonance to be the $1s2l2l'^2L$ or $1s2l3l'^2L$ states. Most of the $1s2l2l'$ states have been studied theoretically in the past with saddle-point and saddle-point complex-rotation methods [20,21]. However, recent improvements in theory, such as the implementation of the restricted variation method, allow us to improve the previous theoretical data substantially. In the case of the lithium atom, recently obtained results agree with precision experiments [22,23] to a few cm^{-1} [24]. Thus we have recalculated these resonances using the improved theoretical methods.

We use the saddle-point variation method in the LS-coupling scheme to calculate the nonrelativistic energy. The nonrelativistic Hamiltonian is given by

$$H_0 = \sum_{i=1}^{N} \left[-\frac{1}{2}\nabla_i^2 - \frac{Z}{r_i} \right] + \sum_{\substack{i,j=1 \\ i<j}}^{N} \frac{1}{r_{ij}}. \tag{3}$$

Multiconfiguration-interaction basis functions are used for the wave function similar to that used by Chung [25]. The proper $1s$ vacancy is built into the wave function with the saddle-point technique. A basic wave function Ψ_b is obtained by optimizing

$$\delta E_b = \delta \frac{\langle \Psi_b | H_0 | \Psi_b \rangle}{\langle \Psi_b | \Psi_b \rangle} = 0. \tag{4}$$

About 600–1000 terms are contained by Ψ_b. The nonlinear parameters in the basis functions are also optimized. To further saturate the functional space, we use the restricted variation method [26]. A more accurate wave function is given by

$$\Psi(1,2,3) = d_0 \Psi_b + \sum_i d_i \Phi_i(1,2,3). \tag{5}$$

The d's are linear parameters that can be determined by a variation calculation in which the Ψ_b from Eq. (4) is treated as a single term. In Eq. (5) the Φ_i's are basis functions similar to those of Ψ_b, but with different nonlinear parameters. The advantage of this method is that in computation it avoids the numerical instability caused by the linear dependence between the basis functions in Ψ_b and Φ_i. For each resonance, we carry out a number of calculations with mutually orthogonal $\Phi_i(1,2,3)$'s. The improvement over E_b is recorded for each calculation. The sum of these improvements ΔE_{RV} gives the total correction from the restricted variation method. The sum of E_b and ΔE_{RV} gives the nonrelativistic saddle-point energy, which represent the best closed-channel approximation to the resonance.

To locate the true resonance, we carry out a complex-rotation calculation using the basis functions in Ψ_b similar to those used by Chen and Chung [24]. The wave function for the complex-rotation calculation is given by

$$\Psi(1,2,3) = \Psi_b(1,2,3) + A\phi_{1s1s}(1,2)U(3), \tag{6}$$

where

$$U(\mathbf{r}) = \sum_n c_n r^n \exp(-\alpha r) Y_{l,m}(\Omega). \tag{7}$$

Here A is the antisymmetrization operator, the c_n's are linear parameters, and α is a nonlinear parameter. The nonlinear parameters in Ψ_b are fixed from the saddle-point calculation. The linear parameters in Ψ_b are allowed to vary in the complex-rotation calculation. The function ϕ_{1s1s} is a 31-term, 4-angular-component wave function for the C V $1s1s$ state with a nonrelativistic energy of $-32.404\,441$ a.u. This $1s1s$ wave function is sufficiently accurate for our purpose since both the width and shift are not very sensitive to the precision of the two-electron target wave function.

In the complex-rotation calculation, only the r in the U part of Ψ is complex scaled. The corresponding complex eigenvalue $E_{\mathrm{res}} - i\Gamma/2$ gives the resonance energy and width for the state. This eigenvalue is stabilized with respect to α and to the rotation angle. The difference $\Delta E_{\mathrm{shift}} = E_{\mathrm{res}} - E_b$ gives the shift from the interaction between the closed channel and open-channel parts of the wave function.

For C IV resonances, the relativistic corrections are very significant. Although the mass polarization effect is very small, the isotope shift could be measured in the future. Hence they are also considered in this work. The perturbation operators are

$$H' = H_1 + H_2 + H_3 + H_4 + H_5, \tag{8}$$

where

$$H_1 = -\frac{1}{M} \sum_{\substack{i,j=1 \\ i<j}}^{3} \nabla_i \cdot \nabla_j \quad \text{(mass polarization)}, \tag{9}$$

$$H_2 = -\frac{1}{8c^2} \sum_{i=1}^{3} \mathbf{p}_i^4 \quad \text{(correction to kinetic energy)}, \tag{10}$$

$$H_3 = \frac{Z\pi}{2c^2} \sum_{i=1}^{3} \delta(\mathbf{r}_i) \quad \text{(Darwin term)}, \tag{11}$$

TABLE I. Energy of the $1s2l2l'$ and $1s2l3l'$ states of C IV (in μa.u.) E_b is the energy calculated from Ψ_b, $\Delta E_{\rm RV}$ is the improvement from the restricted variation calculation, $\Delta E_{\rm MP}$ is the mass polarization energy, $\Delta E_{\rm shift}$ is the shift from the interaction with the continuum, $\Delta E_J = E_{L+1/2} - E_{L-1/2}$ is the fine-structure splitting, and T is the term energy relative to the $1s^2 2s$ in eV.

State	$-E_b$	$-\Delta E_{\rm RV}$	$\Delta E_{\rm shift}$	$\Delta E_{\rm mp}$	$-\Delta E_{\rm rel}$	$-E_{\rm total}$	ΔE_J	T (eV)
$[1s2s2s]^2S$	24 060 477	65	209	-4.4	11 413	24 071 750		291.625
$[1s(2s2p)\ ^3P]^2P^o$	23 754 207	96	435	60.6	10 537	23 764 345	453.4	299.990
$[1s(2s2p)\ ^1P]^2P^o$	23 626 525	134	-12.6	-59.9	10 255	23 636 986	-45.47	303.455
$[1s2p2p]^2D$	23 514 755	124	209	-78.6	9 457	23 524 206	-503.8	306.524
$[1s2p2p]^2P$	23 468 970	60		74.0	9 682	23 478 637	672.1	307.764
$[1s2p2p]^2S$	23 289 429	215	339	-53.8	9 529	23 298 888		312.655
$[1s2s^3S,3s]^2S$	22 453 514	85	39	-5.4	10 703	22 464 268		335.365
$[1s2s^3S,3p]^2P^o$	22 416 004	94	11	4.69	10 487	22 426 569	-142.9	336.391
$[1s2s^3S,3d]^2D$	22 329 742	285	39	76.7	10 549	22 340 360	-36.70	338.737
$[1s2s^1S,3s]^2S$	22 307 359	124	78	12.2	10 198	22 317 592		339.356
$[1s2s^1S,3p]^2P^o$	22 246 453	222	124	-20.4	9 864	22 256 434	98.25	341.021
$[1s2p^3P,3s]^2P^o$	22 197 018	329	189	-52.2	9 560	22 206 770	688.8	342.372
$[1s2s^1S,3d]^2D$	22 167 231	225	21	16.8	9 701	22 177 119	421.4	343.179
$[1s2p^3P,3p]^2D$	22 153 520	297	95	-69.9	9 383	22 163 165	198.9	343.558
$[1s2p^1P,3s]^2P^o$	22 130 263	283	19	67	9 748	22 140 207	-145.7	344.183
$[1s2p^3P,3p]^2S$	22 116 837	221	184	-46.7	9 402	22 126 323		344.561
$[1s2p^3P,3d]^2P^o$	22 083 995	270	5	-72.8	9 194	22 093 527	-298.2	345.453
$[1s2p^1P,3p]^2D$	22 061 570	345	81	53.9	9 529	22 071 310	-75.38	346.058
$[1s2p^1P,3p]^2S$	22 022 953	334	166	48.2	9 610	22 032 676		347.109
$[1s2p^1P,3d]^2P^o$	21 971 305	300	117	74.3	9 448	21 980 862	139.2	348.519

$$H_4 = -\frac{\pi}{c^2}\sum_{\substack{i,j=1\\ i<j}}^{3}\left[1+\frac{8}{3}\mathbf{s}_i\cdot\mathbf{s}_j\right]\delta(\mathbf{r}_{ij})$$
(electron-electron contact term), (12)

$$H_5 = -\frac{1}{2c^2}\sum_{\substack{i,j=1\\ i<j}}^{3}\frac{1}{r_{ij}}\left[\mathbf{p}_i\cdot\mathbf{p}_j+\frac{\mathbf{r}_{ij}(\mathbf{r}_{ij}\cdot\mathbf{p}_i)\cdot\mathbf{p}_j}{r_{ij}^2}\right]$$
(orbit-orbit interaction), (13)

and M is the nuclear mass of ^{12}C.

We have also calculated the fine-structure splitting of the resonance using the spin-orbit and spin-other-orbit operators. They are given by

$$H_{\rm s.o.} = \frac{Z}{2c^2}\sum_{i=1}^{3}\frac{\boldsymbol{l}_i\cdot\mathbf{s}_i}{r_i^3} \quad \text{(spin-orbit)}, \tag{14}$$

$$H_{\rm s.o.o.} = -\frac{1}{2c^2}\sum_{i\neq j}^{3}\left[\frac{1}{r_{ij}^3}(\mathbf{r}_i-\mathbf{r}_j)\times\mathbf{p}_i\right]\cdot(\mathbf{s}_i+2\mathbf{s}_j)$$
(spin-other-orbit). (15)

In Table I we present results for the six $1s2l2l'^2L$ and fourteen $1s2l3l'^2L$ states. Here E_b is the energy from Ψ_b and $\Delta E_{\rm RV}$ is the total improvement from the restricted variation calculation. For some systems such as $1s2p2p\ ^2S$, the angular component converges slowly. Although we include l up to 9 in Ψ_b, the convergence pattern suggests that the higher angular momentum components still contribute. These contributions from the higher-l components are also estimated and included in $\Delta E_{\rm RV}$. Most of the energy shifts $\Delta E_{\rm shift}$ are positive with only one exception, namely, that for the $[1s(2s2p)\ ^1P]\ ^2P^0$ state. Since the mass polarization operator is accurate to all orders, its effect is calculated by including H_1 in H_0 and rediagonalizing the secular equation. The effects due to H_2, H_3, H_4, and H_5 are combined into $\Delta E_{\rm rel}$. They are calculated with first-order perturbation theory. The energy $E_{\rm total}$ is the final result of the resonance energy by including all the effects considered in this work. ΔE_J is the fine-structure splitting of the doublet states. The quantity T in the table is the center-of-gravity energy above the $1s^2 2s$ at $-34.789\,278$ a.u. [27] using 1 a.u. $=$ 27.210 15 eV.

In addition to the Auger width, we have also calculated the radiation transition rates using Ψ_b with the dipole-length, dipole-velocity, and dipole-acceleration formulas. The lower states considered are $1s^2 2s$, $1s^2 2p$, $1s^2 3s$, $1s^2 3p$, and $1s^2 3d$. Their wave functions are calculated using the full core plus correlation method [27]. Generally speaking, the agreement between the three calculations is good, but not excellent. The reason is that for autoionizing doubly excited states, Ψ_b does not include the open-channel part. Therefore, it is only an approximation. As an example, we present the oscillator results for the $1s2l2l'\ ^2L$ states in Table II. In this table we can see that for $[1s2p2p]\ ^2P$, which is a bound state in the nonrelativistic limit, the results of f_l, f_v, and f_a agree quite well. For other states, the agreement between f_v and f_a is better. This could be because the length formula emphasizes the large distance where the open-channel continuum is more significant. Hence we will use the dipole-velocity results to compute transition rates.

TABLE II. Absorption oscillator strength f for the $1s2l2l'^2L-1s^22l''$ transition of C IV. The number in square brackets denotes the power of 10 by which the preceding term is to be multiplied.

State	f_l	f_v	f_a
		$1s^22p$	
$[1s2s2s]^2S$	4.127[-3]	3.514[-3]	3.410[-3]
$[1s2p2p]^2S$	2.637[-2]	2.546[-2]	2.527[-2]
$[1s2p2p]^2P$	2.810[-1]	2.812[-1]	2.811[-1]
$[1s2p2p]^2D$	1.533[-1]	1.505[-1]	1.510[-1]
		$1s^22s$	
$[1s(2s2p)\,^3P,2p]^2P^o$	5.293[-1]	5.150[-1]	5.120[-1]
$[1s(2s2p)\,^1P,2p]^2P^o$	5.144[-2]	5.467[-2]	5.634[-2]

In Table III we present transition rate and lifetime results for the doubly excited states calculated in this work. Both the Auger width and the radiation branching ratios are presented. Since $[1s2p2p]\,^2P$ does not autoionize in the nonrelativistic limit, the radiative branching ratio is 100% and therefore it will not appear in the observed recombination spectra.

IV. RESULTS AND DISCUSSION

The general characteristics of the energy spectrum of doubly excited Li-like carbon can be understood from some basic considerations. He-like carbon has four states with an electron excited to the $n=2$ level. These are $1s2s\,^3S$, $1s2s\,^1S$, $1s2p\,^3P$ and $1s2p\,^1P$, which appear energetically in this order. Series of doubly excited states $1s2snl\,^2L$ and $1s2pnl\,^2L$ in Li-like carbon will converge towards these He-like levels, which will act as series limits. Which state acts as the series limit depends on the core symmetry of the doubly excited state.

The binding energy of a $2s$ electron to the $1s^2$ core of He-like carbon is 64.5 eV, while the binding energy of a $2s$ electron to the $1s$ core in H-like carbon is about 90 eV. Thus we can expect that the binding energy of a $2s$ electron to the *excited* He-like state $1s2s\,^3S$ is somewhere in between. Since the excitation energy of $1s2s\,^3S$ is 299 eV one could expect the lowest doubly-excited state $1s2s^2\,^2S$ to lie about 220 eV above threshold. Our accurate calculations show that it is situated 227.131 eV above threshold. The doubly excited states related to the $n=2$ level in He-like carbon will thus appear in an energy window between 227 eV and 308 eV, the latter being the excitation energy of the $1s2p\,^1P$. There will naturally also be doubly excited levels related to higher-n levels, but they will be harder to observe experimentally. In the present work some spectral features were observed related to the $n=3$ level, but these have not yet been identified.

Experimental observations of doubly excited states are restricted to certain state symmetries, that depend on the type of experimental technique used. Optical emission studies are restricted to states that are forbidden to autoionize or for which autoionization is weak relative to radiative decay. In photoabsorption studies from the ground state, only states of the opposite parity and states differing with no more than one unit of total angular momentum can be observed. For

TABLE III. Autoionization and transition rates for the $1s2l2l'$ and $1s2l3l'$ states of C IV. Γ is the Auger width in meV, η_R is the percentage branching ratio for radiation, and τ is the lifetime of the state. The transition rates W are in sec^{-1} and are calculated with the dipole-velocity formula. The number in square brackets denotes the power of 10 by which the preceding term is to be multiplied.

State	W_{1s^22p}	W_{1s^23p}	W_R	Γ (meV)	η_R(%)	τ (10^{-14} sec)
$[1s2s2s]^2S$	3.678[10]	5.904[8]	3.73[10]	68.02	0.036	0.967
$[1s2p2p]^2S$	3.074[11]	1.195[9]	3.09[11]	7.857	2.52	8.17
$[1s2p2p]^2P$	1.096[12]	5.234[9]	1.10[12]		100	90.9
$[1s2p2p]^2D$	3.489[11]	2.791[9]	3.51[11]	51.23	0.45	1.28
$[1s2s^3S,3s]^2S$	5.312[9]	2.399[8]	5.55[9]	17.62	0.021	3.73
$[1s2s^3S,3d]^2D$	1.507[10]	2.678[8]	1.53[10]	2.358	0.43	27.8
$[1s2s^1S,3s]^2S$	1.289[10]	6.630[10]	7.92[10]	9.666	0.54	6.77
$[1s2s^1S,3d]^2D$	7.403[10]	1.171[11]	1.91[11]	0.663	15.9	83.5
$[1s2p^3P,3p]^2D$	8.865[10]	2.292[9]	9.09[10]	8.968	0.66	7.29
$[1s2p^3P,3p]^2S$	1.798[11]	6.098[10]	2.41[11]	3.065	4.92	20.4
$[1s2p^1P,3p]^2D$	6.995[10]	6.689[11]	7.39[11]	9.562	4.84	6.55
$[1s2p^1P,3p]^2S$	4.098[10]	6.336[11]	6.75[11]	5.515	7.46	11.0

State	W_{1s^22s}	W_{1s^23s}	W_{1s^23d}	W_R	Γ (meV)	η_R (%)	τ (10^{-14} sec)
$[1s(2s2p)^3P]^2P^o$	6.700[11]	1.813[9]	9.243[7]	6.72[11]	3.88	10.2	15.2
$[1s(2s2p)^1P]^2P^o$	7.278[10]	3.865[8]	9.842[8]	7.41[10]	39.91	0.12	1.65
$[1s2s^3S,3p]^2P^o$	1.244[11]	5.116[9]	8.853[7]	1.30[11]	0.550	13.5	104
$[1s2s^1S,3p]^2P^o$	5.581[10]	3.985[10]	2.336[10]	1.19[11]	0.0950	45.2	380
$[1s2p^3P,3s]^2P^o$	1.487[9]	6.193[10]	1.513[9]	6.49[10]	13.89	0.37	4.72
$[1s2p^1P,3s]^2P^o$	2.037[10]	6.526[11]	3.849[10]	7.12[11]	1.460	3.11	43.7
$[1s2p^3P,3d]^2P^o$	1.166[8]	6.586[10]	5.511[9]	7.15[10]	0.176	21.1	295
$[1s2p^1P,3d]^2P^o$	5.790[9]	1.018[10]	7.751[11]	7.91[11]	0.201	72.1	91.2

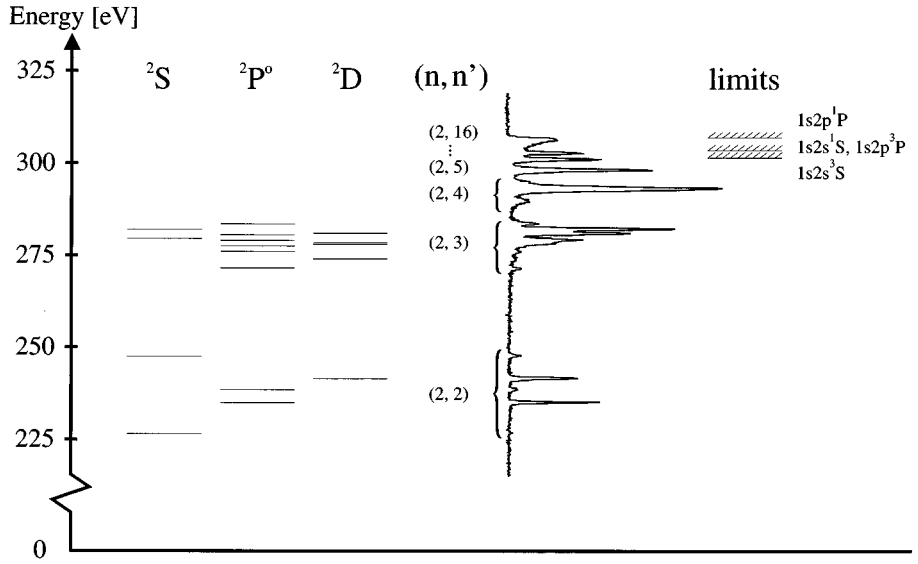

FIG. 1. Partial energy-level diagram for the doubly excited states in C IV (with $n=2$, $n'=2$ and $n=2$, $n'=3$), which are populated by dielectronic recombination. The spectrum obtained in the present experiment is shown as a projection of the continuum on the energy axis with zero set at the ionization threshold of C IV. The first excited states of C V, which act as series limits for the continuum states, are indicated.

dielectronic recombination, which was used in the present experiment, there are different restrictions. The dielectronic recombination process is the inverse of autoionization and consequently only autoionizing states can be observed here. But to complete the recombination, the doubly excited state has to relax by radiative decay. Thus, in DR the critical state-dependent quantity which governs the intensity of the DR peaks is given by a product of the autoionization rate and the radiative rate divided by the sum of the different decay rates. For $A_a \gg A_r$, the DR intensities will be proportional to the radiative transition rate. Consequently, in the present investigation utilizing the dielectronic recombination process, only autoionizing states with open radiative decay channels will be observed. Furthermore, only Rydberg states with principle quantum number smaller than 16 will survive passage of the bending magnet behind the electron target (cf. Sec. II) and this will give a cutoff in the observed Rydberg series progression.

In Fig. 1 the experimental DR spectrum is shown as a projection of the continuum states that are active in the dielectronic recombination process. The cutoff of the Rydberg series is clearly seen at the high-energy end of the spectrum at the $1s2p\ ^1P$ limit, with the typical asymmetric spectral feature. At first one might expect similar cutoff features for the other series limits $1s2s\ ^3S$, $1s2s\ ^1S$, and $1s2s\ ^3P$. There are peaks close to the expected energy positions, but they are symmetric. In a total interpretation of the spectrum, these two peaks find their explanation as members of the Rydberg series approaching $1s2p\ ^1P$. If the other series limits are present, they are hidden in the Rydberg peaks. The weakness of the other series approaching the other series limits ($1s2s\ ^3S$, $1s2s\ ^1S$, and $1s2s\ ^3P$) and the fact that the limits cannot be observed can be understood from the selection rules for the radiative transitions. The core of the doubly excited state has a configuration that is the same as the series limits configuration in its LS term. The radiative relaxation channel for the doubly excited state is primarily determined by a radiative transition of the core. Thus only the $1s2p\ ^1P$ term has an allowed transition channel to $1s^2\ ^1S$. This is the reason why the resonances with a $1s2p\ ^1P$ core are so strong and that this term gives the only observable series limit. The fact that there are still resonances with other cores contributing to the lower-energy part of the spectrum is due to the strong correlation in the doubly excited states observed, which means that LS coupling is not a very good approximation and the LS selection rules for radiative transitions may be violated.

There is, however, another indication of the other series limits in the recorded spectrum. We observe the series approaching $1s2p\ ^1P$ with peaks with principal quantum numbers identified up to $n=7$. Then we note a sudden intensity drop followed by gradual unresolved intensity increase to the series limit (cf. Fig. 2). The sudden intensity drop is explained by the fact that the other series limits have been exceeded, which implies that new continua are opened to which the doubly excited state can autoionize with a high probability, thus reducing the number of recombined ions. This is, in particular, important for the $1s2s\ ^1S$ and the $1s2s\ ^3P$ limits, which lie at the energy of the $n=7$ reso-

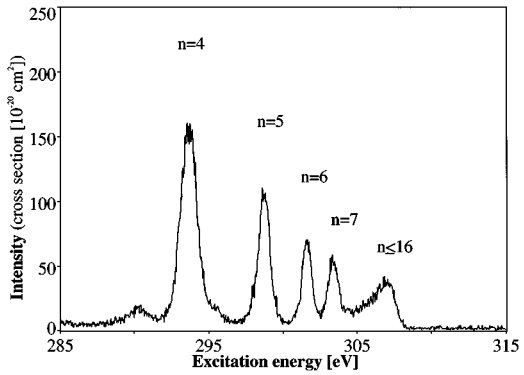

FIG. 2. Highest part of the recorded DR spectrum. Unresolved peaks for dielectronic recombination resonances related to higher principal quantum numbers ($n=2$, $n'>3$). Observe the sudden drop of intensity at $n=8$ due to the appearance of an excited state in helium-like carbon as discussed in the text. The cutoff at $n=16$ in the recorded spectrum is due to field ionization in the motional electric field in the bending magnet behind the electron cooler.

TABLE IV. Excitation energies relative to the ionization limit ($1s^2\ ^1S$) in eV for doubly excited states in C IV.

State	Theory	Experiment			
	This work	This work	Ref. [6]	Ref. [7]	Ref. [10]
$1s2s^2\ ^2S$	227.130	227.10(9)			227.1
$1s(2s2p\ ^3P)\ ^2P^o$	235.495	235.49(1)	235.42	235.42	235.5
$1s(2s2p\ ^1P)\ ^2P^o$	238.960	238.99(2)	239.95	239.28	238.9
$1s2p^2\ ^2D$	242.029	242.05(1)	241.93	242.05	242.0
$1s2p^2\ ^2P$	243.269		243.22		
$1s2p^2\ ^2S$	248.160	248.18(2)			248.2
$(1s2s\ ^3S)3p\ ^2P^o$	271.896	271.87(2)			271.8
$(1s2s\ ^3S)3d\ ^2D$	274.242	274.39(4)			274.2
$(1s2s\ ^1S)3p\ ^2P^o$	276.526	276.57(2)			276.4
$(1s2p\ ^3P)3s\ ^2P^o$	277.877	277.81(3)			277.7
$(1s2s\ ^1S)3d\ ^2D$	278.684	278.60(4)			278.9
$(1s2p\ ^3P)3p\ ^2D$	279.063	279.10(7)			
$(1s2p\ ^1P)3s\ ^2P^o$	279.688	279.68(5)			
$(1s2p\ ^3P)3p\ ^2S$	280.066	280.14(7)			
$(1s2p\ ^3P)3d\ ^2P^o$	280.958	281.05(4)			280.9
$(1s2p\ ^1P)3p\ ^2D$	281.563	281.59(1)			281.4
$(1s2p\ ^1P)3p\ ^2S$	282.614	282.69(1)			282.6
$(1s2p\ ^1P)3d\ ^2P^o$	284.024	284.10(1)			

nance. This conclusion is also confirmed by the experiment of Andersen *et al.* [11], in which a strong Rydberg series is observed approaching 3.5 eV and a weaker series approaching 8.9 eV (cf. their Fig. 9). These energies correspond to the energy differences between the series limits. Thus, in our experiment the high-energy electron recombines by exciting the core, but the electron is readily released with very low kinetic energy leaving the core excited. The opening of new continuum channels was treated theoretically in the work by Kilgus *et al.* [12].

As mentioned in the Introduction, the present work was aimed at obtaining accurate values for excitation energies for doubly excited states in C IV. In Table IV we have collected the theoretical results together with the DR results of this work. Furthermore, we have included accurate spectroscopic values from optical measurements [6,7] and electron spectroscopy [10]. The energies obtained from the DR work by Kilgus *et al.* [12] are not included in the table. Mann [10] claims an uncertainty of 0.1 eV for the energy scale and gives an error of 0.2 eV for the peak position. Nicolosi and Tondello [7] give an uncertainty of 0.01 Å, which corresponds to an energy error of 0.07 eV. Peacock *et al.* [6] do not give error bars, but it might be fair to assume that they have the same error bars as Nicolosi and Tondello. Our experimental uncertainty is not easily estimated. The problem is to establish the energies on an absolute scale since this is determined in the laboratory to center-of-mass transformation. The criteria to be fulfilled in this transformation are discussed in Sec. II. The peak-fitting procedure gives statistical errors, which in our case vary between 0.01 and 0.09 eV. As always in fitting procedures the error estimates are valid provided that the steer data and and boundary conditions are given correctly. Our statistical errors should be valid for relative peak positions within the spectrum. Since this accuracy is much higher than for earlier experimental investigations, it is hard to obtain check points. However, since the high-precision theoretical results are so consistent with our experimental data and also with previous experimental results, we are motivated to use these theoretical results to estimate the accuracy of the determination of the energy scale on an absolute scale. From such a comparison we conclude that this uncertainty is about 0.05 eV. In the table we have chosen not to include this error, which cannot be estimated strictly on experimental grounds.

It should be noted that in the theoretical treatment, the binding energy is calculated, while it is the kinetic energy of the impinging electron (or ejected electron for Auger spectroscopy) that is measured in the experiment. Consequently, it is necessary to relate these numbers in an accurate way for the comparison. In the present work, the calculated value for the binding energy of the ground state ($1s^2 2s\ ^2S$) is $-34.789\,278$ a.u. (1 a.u.$=27.210\,15$ eV). The binding energy of, for instance, $1s2s^2\ ^2S$ is found to be -24.071750 a.u., implying that the excitation energy is 291.625 eV above the ground state. The kinetic energy recorded in the present experiment is then this excitation energy with the ionization potential subtracted. The most accurate value for this quantity has been obtained by Bockasten [28] using classical spectroscopy. He obtained an ionization energy of 64.494 eV, which means that the Auger energy of the $1s2s^2\ ^2S$ state is 227.131 eV. If we refer to the accurate calculated binding energy for $1s^2\ ^1S$ obtained by Pekeris [29] instead of the experimental ionization energy, we obtain a minor difference of 0.7 meV, which is of no significance for the comparison between theory and experiment in the present work. We have, however, chosen to base the theoretical values only on the calculated values and use the value of Pekeris [29]. The theoretical energy for $1s2s^2\ ^2S$ is consequently 227.130 eV. The energies of the excited He-like carbon states, which act

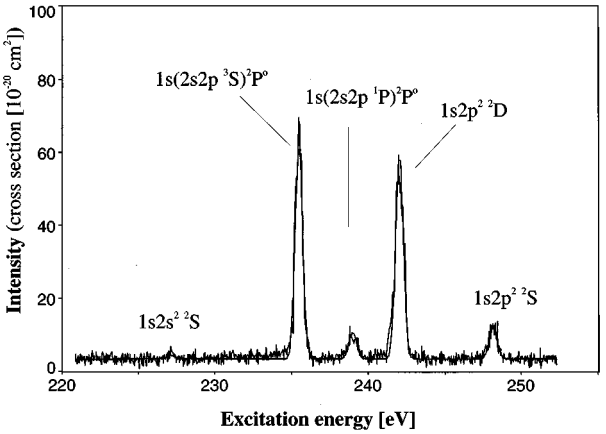

FIG. 3. Lowest part of the DR spectrum of lithiumlike carbon containing resonances for which both outer electrons have principal quantum number $n=2$. Doubly excited states are given in LS notation. Observe that no trace of the $1s2p^2\,{}^2P$ state at 243.2 eV is seen, in accordance with the selection rules for dielectronic recombination. The fitted function of asymmetric DR resonances is superimposed.

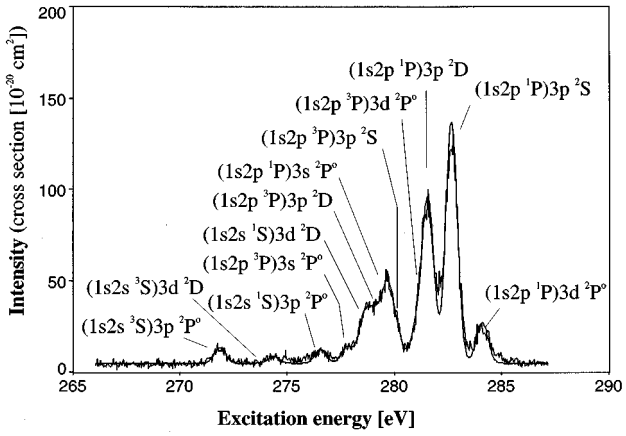

FIG. 4. Recorded ($n=2$, $n'=3$) DR resonances. The intensity is given as the cross section for dielectronic recombination.

as series limits, have been obtained from the experimental work of Engström *et al.* [30]. These are 298.962 eV for $1s2s\ {}^3S$, 304.387 eV for $1s2s\ {}^1S$, 304.412 eV for $1s2p\ {}^3P$ (weighted average for the fine structure multiplet), and 307.901 eV for $1s2p\ {}^1P$.

The $1s2s^2\,{}^2S$ state might not be expected to be observed in a DR spectrum since this state has no allowed radiative decay channel. As found by the calculation (Table III), this state has, however, an appreciable radiative decay rate, only a factor 10–30 smaller than other resonances. This is due to the strong correlation that mixes the state with the $1s2p^2\,{}^2S$ state. At a close inspection of the spectrum a very weak line is observed (Fig. 3), with an energy that is in very good agreement with the theoretical value. The fact that the multiplicity of the ^2S state is low also suppresses the relative intensity of this peak.

In a comparison with the work of Kilgus *et al.* [12] we note that the resolution in the present spectrum is considerably higher. In the spectral region around 240 eV, where the $n=2$, $n'=2$ resonances lie, the peaks are well resolved and we note that no trace of the $1s2p^2\,{}^2P$ state can be observed. This is in agreement with the basic considerations discussed above. Since there is no continuum of even-parity ^2P in this energy region, neither autoionization nor dielectronic recombination is possible. Such processes could only be possible through relativistic interactions (i.e., spin-dependent interaction), which are very weak here. Though the resolution in this work is much higher than in the earlier measurements, the experimental linewidth is far too large to expose the natural line widths. The largest autoionization widths are for the lowest resonances. According to the calculations (Table III) the autoionization width of $1s2s^2\,{}^2S$ is 68 meV and for $1s2p^2\,{}^2D$ 51 meV, which is about one order of magnitude smaller than the experimental linewidth. For higher principal quantum numbers the autoionization width will be smaller (due to weaker electron-electron Coulomb interaction). The width of the $1s2p^2\,{}^2D$ state has been determined for the preceding members of the isoelectronic sequence by optical measurements [2]. In Li I the width is 10.5 ± 0.3 meV [22], in Be II 30.3 ± 1.1 meV [31], and in B III 42 ± 4 meV [32]. The present calculated value for C IV (51 meV) follows the general pattern. Only a weak dependence on Z is expected for the autoionization widths.

Many of the $n=2$, $n'=3$ resonances are well resolved (Fig. 4). As can be seen in Table IV, every resonance to be expected is indeed observed. There is one particular spectral feature at about 280 eV, for which the limited experimental resolution causes difficulties. The theoretical calculations and the experimental analysis were initially performed in a double blind procedure, meaning that they were performed independently without knowledge of each other's results. The theoretical results obtained in this way are those presented in the tables of the present article. The independent peak fitting analysis gave results essentially the same as given in the table. For the region discussed here at about 280 eV, the two peaks for the $(1s2p\ {}^3P)3p\ {}^2S$ and

TABLE V. Integrated cross sections for individual resonances in C IV observed in the present experiment.

	Integrated cross section (10^{-21} cm^2 eV)			
	Experiment		Theory	
State	This work	Ref. [12]	Ref. [33]	Ref. [12]
$1s2s^2\,{}^2S$	0.7(0.2)			
$1s(2s2p\ {}^3P)\ {}^2P^o$	39.3(6)	39.3(9)	39.0	44.1
$1s(2s2p^1P)\ {}^2P^o$	4.9(3)	6.1(6)	13.2	5.4
$1s2p^2\,{}^2D$	37.2(6)	34.5(8)	42.2	37.8
$1s2p^2\,{}^2S$	5.9(3)	5.6(5)	8.4	7.6
$(1s2s\ {}^3S)3p\ {}^2P^o$	5.7(3)		7.7	
$(1s2s\ {}^3S)3d\ {}^2D$	2.5(3)			
$(1s2s\ {}^1S)3p\ {}^2P^o$	5.1(3)		2.5	
$(1s2p\ {}^3P)3s\ {}^2P^o$	6.0(3)		31.3	
$(1s2s\ {}^1S)3d\ {}^2D$	16.2(6)			
$(1s2p\ {}^3P)3p\ {}^2D$	16.2(7)		11.3	
$(1s2p\ {}^1P)3s\ {}^2P^o$	27.1(7)		11.2	
$(1s2p\ {}^3P)3p\ {}^2S$	9.5(6)		2.7	
$(1s2p\ {}^3P)3d\ {}^2P^o$	12.8(6)		7.8	
$(1s2p\ {}^1P)3p\ {}^2D$	60.0(9)		21.8	
$(1s2p\ {}^1P)3p\ {}^2S$	89.0(10)		4.3	
$(1s2p\ {}^1P)3d\ {}^2P^o$	15.0(4)		1.3	

$(1s2p\ ^3P)3d\ ^2P^o$ states at 280.066 and 281.000 eV, respectively, according to theory, were not detected in the analysis since they are lying in the wing of the strong lines. Omission of these lines caused the lines corresponding to $(1s2p\ ^3P)3p\ ^2D$ and $(1s2p\ ^1P)3s\ ^2P^o$ at 279.064 and 279.690 eV, respectively, to be moved to slightly higher values (by about 0.15 eV). This is natural since in the peak fitting procedure, these peaks had to compensate for the intensity of the 280.066 eV line not included in the fit. Thus this part of the region was reanalyzed with the $(1s2p\ ^3P)3p\ ^2S$ and $(1s2p\ ^3P)3d\ ^2P^o$ peaks included. The quality of the fit as measured by the χ^2 was significantly improved and the energies of all four peaks discussed here were converging to values in good agreement with theory.

For the peaks at higher energies (above 290 eV) no detailed position determination has been performed since the resolution is too low to distinguish resonances of $n=2$, $n'>3$ from each other. Spectral clusters of similar appearance as that between 272 and 284 eV should be expected for higher principal quantum numbers n'. Separate peaks for every $n'=4-7$ are observed as discussed earlier in this section. The main contribution comes from $(1s2p\ ^1P)n'p\ ^2S$ in each peak, but there are also unresolved contributions from other resonances such as $(1s2p\ ^1P)n's\ ^2P^o$, $(1s2p\ ^1P)n'p\ ^2D$, and $(1s2p\ ^1P)n'd\ ^2P^o$.

Although the goal for the present experiment was to accurately determine excitation energies for resonant states, we also include a table of cross sections for the different resonances. These are given in terms of integrated cross sections for the energy profile of the resonances. In Table V these cross sections are given and compared with the experimental and theoretical results of Kilgus *et al.* [12]. The theoretical results obtained by Bellantone and Hahn [33] are also included. Very large discrepancies were found for the $(1s2p\ ^3P)3s\ ^2P^o$, $(1s2p\ ^1P)3p\ ^2S$, and $(1s2p\ ^1P)3d\ ^2P^o$, states for which $\sigma_{\rm expt}/\sigma_{\rm theor}$ are 0.19, 21, and 12, respectively. For other states the disagreement is not as large and the experimental and theoretical values agree within a factor 2–3.

V. CONCLUSION

The present work shows that an electron cooler at an ion storage ring can be used to perform precision spectroscopy of autoionizing states with an unprecedented accuracy, even though the determination of the energies on an absolute scale is difficult, in particular at the high excitation energies studied here. The method is also clean from contributions from other charge states, which can be harmful in other techniques. In the present experiment we also observe that high kinetic energy is converted to very low energy by dielectronic recombination followed by autoionization. The energy is absorbed by the target ion, which will release the energy in form of a high energy photon.

It is also shown that the available theoretical method that employs the saddle-point technique, is capable of very high accuracy. In fact, there is still no experimental results available that are of sufficient quality to test the accuracy of this theoretical treatment. The inherent problems to accurately determine energies for resonant states both for theory and experiment have so far limited the accuracy to orders of magnitude lower than for ordinary bound states. The present work, however, shows that considerable improvements are possible.

ACKNOWLEDGMENTS

We are grateful for very competent support from the Manne Siegbahn Laboratory. We are also grateful to Dr. G. Dunn for valuable comments on the manuscript. This work is supported by the Swedish Natural Science Research Council (NFR). K.T.C. is supported by the National Science Foundation, Grant No. PHY93-14907.

[1] B. Edlén and A. Tyrén, Nature **143**, 940 (1939).
[2] S. Mannervik, Phys. Scr. **40**, 28 (1989).
[3] P.D. Dumont, H.P. Garnir, Y. Baudinet-Robinet, and K.T. Chung, Phys. Rev. A **32**, 229 (1985).
[4] J.H. Blanke, P.H. Heckmann, E. Träbert, and R. Hucke, Phys. Scri. **35**, 780 (1987).
[5] U. Feldman and L. Cohen, Astrophys. J. **158**, L169 (1969).
[6] N.J. Peacock, M.G. Hobby, and M. Galanti, J. Phys. B **6**, L298 (1973).
[7] P. Nicolosi and G. Tondello, J. Opt. Soc. Am. **67**, 1033 (1977).
[8] D. Schneider, R. Bruch, W.H.E. Schwarz, T.C. Chang, and C.F. Moore, Phys. Rev. A **15**, 926 (1977).
[9] M. Rødbro, R. Bruch, and P. Bisgaard, J. Phys. B **12**, 2413 (1979).
[10] R. Mann, Phys. Rev. A **35**, 4988 (1987).
[11] L.H. Andersen, J. Bolko, and P. Kvistgaard, Phys. Rev. A **41**, 1293 (1990).
[12] G. Kilgus, D. Habs, D. Schwalm, A. Wolf, R. Schuch, and N.R. Badnell, Phys. Rev. A **47**, 4859 (1993).
[13] D.R. DeWitt, R. Schuch, T. Quinteros, H. Gao, W. Zong, H. Danared, M. Pajek, and N.R. Badnell, Phys. Rev. A **50**, 1257 (1994).
[14] D.R. DeWitt, E. Lindroth, R. Schuch, H. Gao, T. Quinteros, and W. Zong, J. Phys. B **28**, L147 (1995).
[15] C.F. Bunge, Phys. Rev. A **23**, 2060 (1981).
[16] K.T. Chung, Phys. Rev. A **29**, 682 (1984); J.J. Hsu, K.T. Chung, and K.N. Huang, *ibid.* **44**, 5485 (1991).
[17] K.T. Chung, Phys. Rev. A **20**, 1743 (1979).
[18] K. Abrahamsson *et al.*, Nucl. Instrum. Methods Phys. Res. Sect. B **79**, 269 (1993).
[19] G. Kilgus, D. Habs, D. Schwalm, A. Wolf, N.R. Badnell, and A. Müller, Phys. Rev. A **46**, 5730 (1992).
[20] R. Bruch, K.T. Chung, W.L. Luken, and J.C. Culberson, Phys. Rev. A **31**, 310 (1985).
[21] B.F. Davis and K.T. Chung, Phys. Rev. A **37**, 111 (1988); **39**, 3942 (1989).
[22] H. Cederquist and S. Mannervik, J. Phys. B **15**, L807 (1982).
[23] H. Cederquist and S. Mannervik, Phys. Scr. **31**, 171 (1985).
[24] M.K. Chen and K.T. Chung, Phys. Rev. A **49**, 1675 (1994).
[25] K.T. Chung, Phys. Rev. A **23**, 2957 (1981).
[26] K.T. Chung and X.-W. Zhu, Phys. Scr. **48**, 292 (1993).
[27] K.T. Chung, Phys. Rev. A **44**, 5421 (1991).
[28] K. Bockasten, Ark. Fys. **10**, 567 (1956).
[29] C.L. Pekeris, Phys. Rev. **112**, 1649 (1958).

[30] L. Enström, P. Bengtsson, C. Jupén, and M. Westerlind, J. Phys. B **25**, 2459 (1992).
[31] H. Cederquist, M. Kisielinski, S. Mannervik, and T. Andersen, J. Phys. B **17**, 1969 (1984).
[32] Y. Baudinet-Robinet, H.P. Garnir, and P.D. Dumont, Phys. Rev. A **34**, 4722 (1986).
[33] R. Bellantone and Y. Hahn, Phys. Rev. A **40**, 6913 (1989).